nature COMMUNICATIONS

ARTICLE

Received 19 Apr 2013 | Accepted 23 Aug 2013 | Published 17 Sep 2013

DOI: 10.1038/ncomms3500

Unidirectional suppression of hydrogen oxidation on oxidized platinum clusters

Yu Hang Li[1,*], Jun Xing[1,*], Zong Jia Chen[2], Zhen Li[3], Feng Tian[4], Li Rong Zheng[5], Hai Feng Wang[2], P. Hu[2,6], Hui Jun Zhao[7] & Hua Gui Yang[1,7]

Solar-driven water splitting to produce hydrogen may be an ideal solution for global energy and environment issues. Among the various photocatalytic systems, platinum has been widely used to co-catalyse the reduction of protons in water for hydrogen evolution. However, the undesirable hydrogen oxidation reaction can also be readily catalysed by metallic platinum, which limits the solar energy conversion efficiency in artificial photosynthesis. Here we report that the unidirectional suppression of hydrogen oxidation in photocatalytic water splitting can be fulfilled by controlling the valence state of platinum; this platinum-based cocatalyst in a higher oxidation state can act as an efficient hydrogen evolution site while suppressing the undesirable hydrogen back-oxidation. The findings in this work may pave the way for developing other high-efficientcy platinum-based catalysts for photocatalysis, photoelectrochemistry, fuel cells and water–gas shift reactions.

[1] Key Laboratory for Ultrafine Materials of Ministry of Education, School of Materials Science and Engineering, East China University of Science and Technology, 130 Meilong Road, Shanghai 200237, China. [2] State Key Laboratory of Chemical Engineering, Centre for Computational Chemistry and Research Institute of Industrial Catalysis, East China University of Science and Technology, 130 Meilong Road, Shanghai 200237, China. [3] Institute for Superconducting and Electronic Materials, Australian Institute of Innovative Materials, University of Wollongong, North Wollongong, New South Wales 2500, Australia. [4] School of Materials Science and Engineering, University of Shanghai for Science and Technology, 516 Jungong Road, Shanghai 200093, China. [5] Beijing Synchrotron Radiation Facility, Institute of High Energy Physics, Chinese Academy of Sciences, Beijing 100049, China. [6] School of Chemistry and Chemical Engineering, The Queen's University of Belfast, Belfast BT9 5AG, UK. [7] Centre for Clean Environment and Energy, Gold Coast Campus, Griffith University, Queensland 4222, Australia. * These authors contributed equally to this work. Correspondence and requests for materials should be addressed to H.G.Y. (email: hgyang@ecust.edu.cn) or to H.F.W. (email: hfwang@ecust.edu.cn).

Photocatalytic water splitting is a process for potentially green and renewable hydrogen generation[1–4]. Over the past decades, many revolutionary photocatalysts have been developed, and most of them require cocatalysts to act as active sites for H_2 evolution at their surface[5–9]. To date, various noble metals and semiconductors have been used to cocatalyze water decomposition into hydrogen and oxygen[10], and in particular, metallic platinum nanoparticles (m-Pt NPs) have been widely employed as the cocatalyst with various light-harvesting semiconductors for the hydrogen evolution reaction (HER)[11]. In a photocatalytic system modified with m-Pt NPs cocatalyst, the photoexcited electrons in semiconductors can rapidly transfer to the m-Pt NPs cocatalysts through the metal–semiconductor interface (Schottky layer), and reduce protons (H^+) in an aqueous reaction medium to form H_2 (ref. 12). Unfortunately, hydrogen back-oxidation is also catalysed by metallic Pt cocatalysts because of their robust adsorption property and its low activation energy[13]. This is a classical reaction applied in the proton exchange membrane fuel cell that can convert chemical energy directly into electrical energy[14]. This undesirable back-reaction drastically limits the solar energy conversion efficiency of fuel-reforming catalysts, and it is an open challenge to specifically suppress the undesirable hydrogen oxidation reaction (HOR) while preserving an efficient hydrogen evolution rate in artificial photosynthesis systems[15,16].

Here we find that Pt in a higher oxidation state (that is, PtO) demonstrates remarkable HOR suppression ability, while its hydrogen evolution capacity is still comparable to that of the benchmark of conventional metallic Pt cocatalyst through comprehensive experimental and theoretical analysis (see Fig. 1 for schematic mechanism). This work confirms the role of PtO cocatalyst in governing the preferred direction of H_2 reactions, and the finding may pave the way for developing other high-efficientcy catalysts for water splitting, water–gas shift reactions and fuel cells.

Results

Loading cocatalysts. In a typical cocatalyst loading process, the metallic Pt was loaded on anatase TiO_2{001} nanosheets (Supplementary Fig. S1) through conventional chemical reduction (CCR) method[17], which used sodium borohydride ($NaBH_4$) as reductant that can readily reduce Pt^{4+} precursor into m-Pt NPs (denoted as Pt/TiO_2). On the basis of CCR process, poly(methacrylic acid) ligands; (see Supplementary Note 1 for details; Supplementary Figs S2 and S3) were involved in ligands-assist chemical reduction (LCR) process, which can controllably load pure PtO-clusters cocatalyst with ultrafine particle size and extraordinary stability on the same TiO_2{001} nanosheets (denoted as PtO/TiO_2; see Methods for detailed experimental method). The Pt loading amount of the as-prepared photocatalysts can be tested to be 1.0 wt% for Pt/TiO_2 and 0.5 wt% for PtO/TiO_2 by inductively coupled plasma (ICP)-atomic emission spectroscopy.

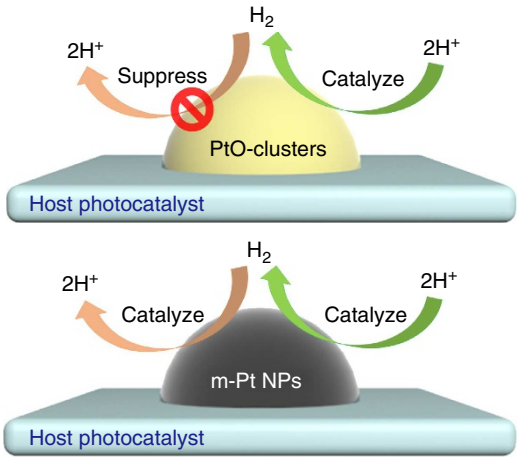

Figure 1 | Schematic photocatalytic H_2 evolution and back-reaction processes. Both PtO-clusters and metallic Pt nanoparticles (m-Pt NPs) cocatalysts can act as H_2 evolution site on host photocatalyst surface, whereas the undesirable H_2 back-reaction can be suppressed by PtO-clusters cocatalyst but facilitated by m-Pt NPs cocatalyst.

Electron microscopy. The geometric morphology of the initial PtO/TiO_2 photocatalyst was first examined by high-resolution transmission electron microscopy (TEM). As illustrated in Supplementary Fig. S4, the photocatalyst has a clean surface and the particle size of the current PtO-clusters (white circles) is extreme small. Interestingly, no apparent diffraction rings of PtO can be observed in selected-area electron diffraction pattern, whereas all diffraction rings can correspond to the host TiO_2 photocatalyst[18], which may owe to the small size and loading amount of the PtO-clusters cocatalyst. Meanwhile, it can be clearly found that the isolated PtO-clusters (bright spots) are uniformly dispersed on TiO_2 surface, as shown in the scanning TEM image (STEM; Fig. 2a), and the particle size distribution of the PtO-clusters (inset of Fig. 2a) reflects that the LCR process can optimize the cocatalyst to be subnanometre-sized cluster, whereas the CCR process demonstrates uncontrollable loading results that show disordered morphology of metallic Pt cocatalyst with a mean particle size around 2 nm (Supplementary Fig. S5). The PtO-clusters are well dispersed over the basal planes and edges of the TiO_2{001} nanosheets, possibly originating from the strong interactions between the surface functional groups and ligand-assisted Pt ions, and subsequently the formation of oxidized Pt. Specifically, according to the STEM characterization, the PtO-cluster is found to usually contain $6 \sim 10$ Pt atoms.

X-ray photoelectron spectroscopy. To examine the chemical state and dispersion of Pt species in both cocatalysts, the PtO/TiO_2 and Pt/TiO_2 photocatalysts were then studied by X-ray photoelectron spectroscopy (XPS; Supplementary Fig. S6). The main peaks in PtO/TiO_2 photocatalyst centre at 72.4 and 75.8 eV, which can be assigned to Pt^{2+} bonded to oxygen[19]. On the other hand, Pt/TiO_2 photocatalyst has two obvious peaks of Pt $4f_{7/2}$ and $4f_{5/2}$ at 70.9 and 74.3 eV, respectively, indicating the existence of the metallic Pt. However, the existence of PtO_2 phase can be safely ruled out because the binding energies of Pt^{4+} $4f_{7/2}$ and $4f_{5/2}$ are 73.8 and 77.1 eV, respectively[20]. Thus, the Pt species in PtO/TiO_2 and Pt/TiO_2 photocatalysts are assigned to PtO and metallic Pt, respectively. Specifically, the dispersion of Pt in both photocatalysts can be evaluated by the relative XPS intensity ratio of Pt atom to Ti atom (I_{Pt}/I_{Ti}; Supplementary Table S1). On the basis of the initial ICP result discussed above, the high value of I_{Pt}/I_{Ti} in PtO/TiO_2 (0.021) demonstrates the excellent dispersion of PtO-clusters on TiO_2 surface, and the low value of I_{Pt}/I_{Ti} in Pt/TiO_2 (0.014) might be caused by the average particle size of metallic Pt that significantly exceeds the electron escape depth[21]. Moreover, XPS analysis suggests that the O 1*s* and Ti 2*p* in two photocatalysts are quite similar (Supplementary Figs S7 and S8), indicating that no conspicuous affection occurred on the surface atomic structures of the host TiO_2 during the cocatalyst loading process. Further, according to high-resolution TEM and XPS analysis, no ligands can be detected in the PtO/TiO_2 photocatalyst, indicating that the ligands used in LCR process have

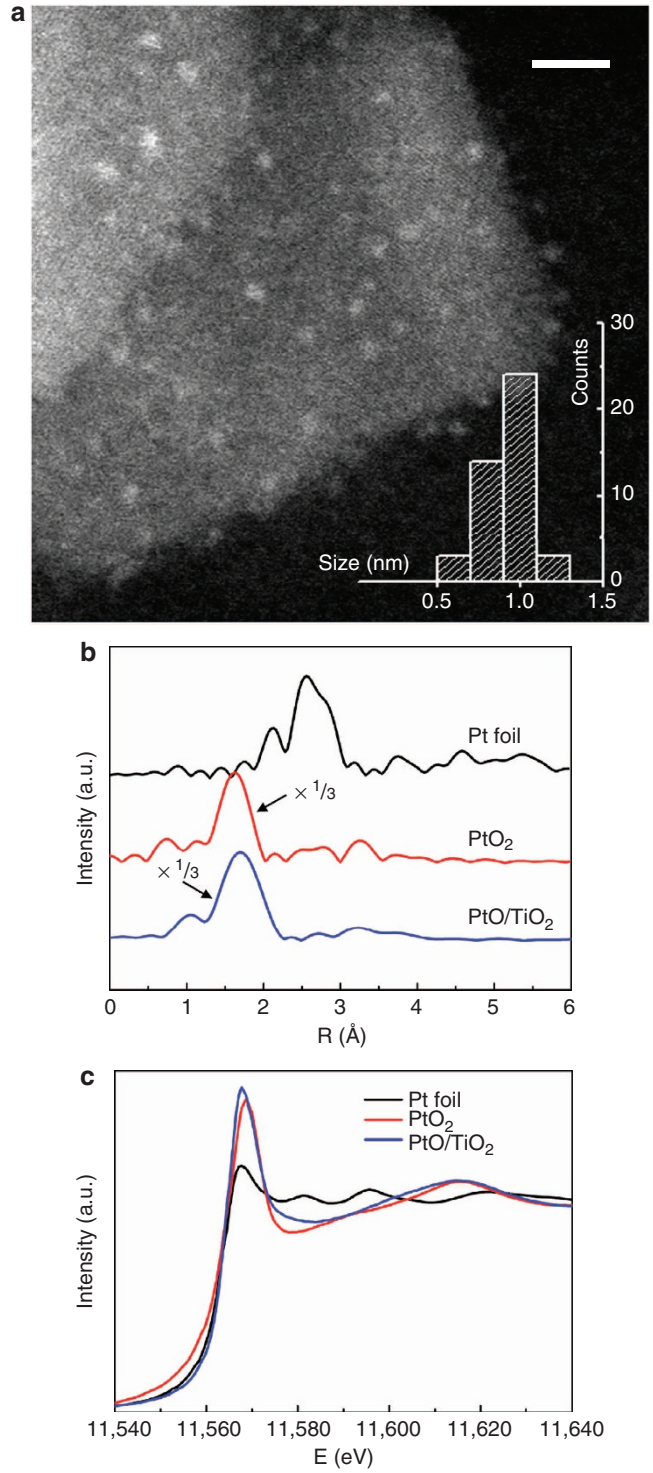

Figure 2 | Structure analyses of initial PtO/TiO_2 photocatalytic system. (**a**) Representative STEM image where isolated three-dimensional PtO-clusters (bright spots) can be observed clearly. The particle size distribution of PtO-clusters cocatalyst is shown in the inset, and the average particle size as estimated from STEM image is 1.0 ± 0.3 nm. Scale bar, 5 nm. (**b**) The k^3-weighted Fourier transform spectra from EXAFS. $\times\frac{1}{3}$ represents signal magnification. (**c**) The normalized X-ray absorption near-edge structure spectra at the Pt L_3-edge of the Pt foil, PtO_2 and initial PtO/TiO_2 photocatalyst.

been completely removed in washing process through the strong intermolecular force with ethanol.

X-ray absorption fine structure studies. Fourier-transformed spectrum of the Pt L_3-edge extended X-ray absorption fine structure (EXAFS) for the PtO/TiO_2 photocatalyst is displayed in Fig. 2b, which shows only one apparent peak at 1.0–2.0 Å. To identify the nature of the backscatterer, EXAFS spectra of Pt and PtO_2 samples were measured as reference. The peak at 1.0–2.0 Å in PtO_2 is because of scattering from the nearest oxygen atoms, whereas the peak at 2.0–3.3 Å in Pt foil is because of scattering from the neighbouring Pt. Thus, the only peak at 1.0–2.0 Å in PtO/TiO_2 is believed to be the contribution from Pt-O binding. Owing to the high disordering in the higher shells, only the main peak in the R ranging from 1.0 to 2.0 Å was considered in the EXAFS curve-fitting (fitting parameters are shown in Supplementary Table S2). There is Pt-O contribution at a distance of 2.07 Å for the PtO/TiO_2 photocatalyst, and the coordination number is 4.0, suggesting the Pt species is the PtO phase, which agrees well with the literature data[22]. Figure 2c shows the normalized X-ray absorption near-edge structure spectrum of PtO/TiO_2 photocatalyst, and the reference spectra of Pt foil and PtO_2. The white-line intensities in the spectra reflect the oxidation state of Pt in different samples. Thus, the white-line intensity of the PtO/TiO_2, which is close to that of PtO_2, further suggests that the Pt in the photocatalyst exists as oxidized Pt. Combined with XPS analysis, it can be concluded that the Pt species in the photocatalyst is the PtO phase.

HOR suppression ability of the PtO-clusters. HOR suppression ability was measured over the as-prepared Pt/TiO_2 and PtO/TiO_2 photocatalysts. In a typical experiment, 50 mg of either photocatalyst was dispersed in 100 ml of deionized water in the reaction vessel. H_2 (2 ml) and O_2 (1 ml) with stoichiometric composition were injected into the closed system before the photocatalytic H_2 evolution test; the gas content was monitored every 15 min via an online gas chromatograph (Fig. 3a). Interestingly, a remarkable decrease of both H_2 and O_2 amount was observed on Pt/TiO_2 photocatalyst, which exhibits negligible photocatalytic activity for pure water splitting even after extended periods of light irradiation, mainly because of the rapid undesirable HOR on m-Pt NPs cocatalyst. However, photocatalyst loaded with the PtO-clusters gave stoichiometric H_2 and O_2 evolution from pure water under ultraviolet–visibile light irradiation. Both H_2 and O_2 evolve steadily and stoichiometrically as the reaction proceeds, indicating that the PtO-clusters cocatalyst demonstrates a remarkable HOR suppression capability. It should be noticed that the photogenerated holes may react with TiO_2 and water to form peroxotitanate complexes at the surface and H_2O_2 in solution[23]. Thus, a photocatalytic test in pure water (100 ml) without adding H_2 and O_2 in the reactor was performed to further confirm the molecular O_2 evolution (Supplementary Fig. S9). The stoichiometric H_2 and O_2 still evolve steadily as the reaction proceeds, indicating that the molecular O_2 (together with H_2) can be evolved in the gas phase through pure water splitting in the current PtO/TiO_2 photocatalytic system. Moreover, the HOR suppression ability was also measured in darkness (Supplementary Fig. S10). A similar decrease of both H_2 and O_2 amount was observed on Pt/TiO_2 photocatalyst, whereas the HOR on PtO/TiO_2 was negligible. Thus, it is clear that water formation from H_2 and O_2 on m-Pt NPs is significant during water-splitting reaction. However, in the PtO/TiO_2 photocatalytic system, the suppression of water formation is significant, which is essential to achieve efficient evolution of H_2 and O_2.

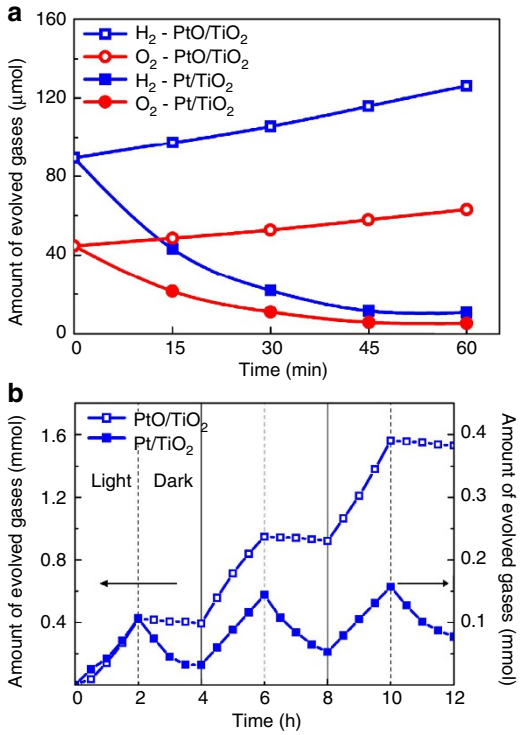

Figure 3 | HOR suppression in photocatalytic H_2 evolution test. (**a**) Reaction time profiles of the HOR with H_2 and O_2 on PtO/TiO_2 and Pt/TiO_2 photocatalysts under ultraviolet–visible light irradiation ($\lambda > 300$ nm). In a typical experiment, 2 ml of H_2 and 1 ml of O_2 were injected into the evacuated system with the time set as 0. (**b**) H_2 evolution and undesirable oxidation in methanol aqueous solution under ultraviolet–visible light irradiation ($\lambda > 300$ nm, 2 h) and followed dark condition (light off, 2 h) for three times on PtO/TiO_2 and Pt/TiO_2. PtO/TiO_2: 219.3 μmol h^{-1} (light), −16.0 μmol h^{-1} (dark); Pt/TiO_2: 53.8 μmol h^{-1} (light), −41.0 μmol h^{-1} (dark).

In addition, the HOR suppression abilities of both photocatalysts were also studied in methanol aqueous solution (100 ml, 30 v/v %). The reaction vessel was initially irradiated for 2 h (light reaction), and then kept in darkness for another 2 h (dark reaction) to observe the H_2 back-reaction. The amounts of H_2 are illustrated in Fig. 3b. In the light reaction, the photocatalytic H_2 evolution activity of PtO/TiO_2 is nearly four times higher than that of Pt/TiO_2, which may be attributed to the ultrafine particle size and high dispersion of PtO-clusters compared with that of m-Pt NPs loaded on TiO_2. Interestingly, in the dark reaction, the pressures of H_2 on the Pt/TiO_2 photocatalyst decreased very quickly, whereas those on PtO/TiO_2 decreased negligibly, which show the same tendencies with respect to the results in pure water system. The inactivity of the PtO-clusters cocatalyst for the undesirable H_2 back-reaction can be a positive characteristic for photocatalytic H_2 generation. The reaction rate ratio of H_2 decrease (dark reaction) to H_2 evolution (light reaction) on PtO/TiO_2 photocatalyst is merely 10 %, whereas that on Pt/TiO_2 drastically climbs to 80 %. Accordingly, in the current PtO/TiO_2 photocatalytic system, the PtO-clusters cocatalyst does govern the favourite direction of H_2 reactions, and can be considered to have two roles: (i) acting as efficient H_2 evolution sites on host photocatalyst surface and (ii) suppressing the undesirable H_2 back-reaction.

Photochemical stability as well as photocatalytic activity is crucial factor for a practical photocatalyst. The conventional oxidized Pt species can be reduced to metallic Pt by the photo-excited electrons during photocatalytic tests, especially in methanol aqueous solution[24,25]. Therefore, the structure of PtO/TiO_2 photocatalyst was again studied by STEM, XPS and EXAFS analyses after photocatalytic test in methanol aqueous solution. The geometric morphology of PtO/TiO_2 photocatalyst (Supplementary Fig. S11) still exhibits subnanometre PtO-clusters attached on the host photocatalyst surface, suggesting that the isolated PtO-cluster retains excellent structure stability. Moreover, the Pt 4*f* XPS spectra and the I_{Pt}/I_{Ti} were detected with negligible difference between the initial and used PtO/TiO_2 photocatalyst (Supplementary Fig. S12 and Supplementary Table S1), and the EXAFS spectra show that the used photocatalyst still has only one apparent peak at 1.0–2.0 Å, suggesting that the Pt species in the used photocatalyst remains as the PtO phase (Supplementary Fig. S13). In addition, the life cycle measurement in methanol aqueous solution was carried out to confirm the photocatalytic stability of the PtO/TiO_2 photocatalyst (Supplementary Fig. S14). The PtO/TiO_2 showed good durability for 6 days of operation under ultraviolet–visible light irradiation. Further, the stability of the PtO/TiO_2 photocatalyst was also explored by virtue of density functional theory (DFT) calculations (Supplementary Figs S15 and S16, Supplementary Table S3). All results strongly suggest that PtO-clusters cocatalyst we prepared has an excellent stability.

DFT studies. To demonstrate the relative activity of the oxidized PtO species and metallic Pt cocatalyst in affecting HOR, we investigated the detailed pathways of H_2 reacting with O_2 ($H_2 + 1/2O_2 \rightarrow H_2O$) occurring on these two kinds of catalysts by virtue of DFT calculations (see calculation details in Methods). To simulate the oxidized PtO-clusters cocatalyst, Pt_8O_8-cluster supported by TiO_2(001) surface (Pt_8O_8/TiO_2) was selected on the account of the experimental STEM characterization (Fig. 2a), which indicates the PtO cluster usually containing 6 ~ 10 Pt atoms, whereas for the metallic Pt cluster on TiO_2(001) surface, Pt_{12} cluster (Pt_{12}/TiO_2) was tested and selected (see details in Supplementary Table S4), in which the molecular dynamics simulation was applied to screen the optimal structure (Fig. 4a–c). The common elementary reaction steps involved in HOR on metal Pt surfaces contain (i) adsorption and dissociation of H_2 and O_2 molecule and (ii) the surface O* reacting with H* into OH*, and further to H_2O. Alternatively, the formation of surface OH* could be accomplished through surface O* reacting with one H_2O molecule, instead of the direct coupling of surface H* and O* atoms[26,27]. As shown in Table 1, reaction barriers and Gibbs free energy changes of these elementary steps on both Pt_{12}/TiO_2 and Pt_8O_8/TiO_2 were calculated (see structures in Supplementary Figs S17–S20 and adsorption energies in Supplementary Table S4). On Pt_{12}/TiO_2, it is found that O_2 molecule has a large adsorption energy of −1.67 eV (with the gas-phase entropy of O_2 at 298 K included), and the adsorbed O_2* can easily dissociate into two atomic O* with a large energy gain of 1.51 eV and a barrier as low as 0.49 eV. Meanwhile, H_2 molecule can even directly dissociate into atomic H* on adsorption at Pt_{12}/TiO_2 with a large Gibbs free energy gain of 1.06 eV. Therefore, it can be concluded that H_2 and O_2 can be easily activated in the presence of metallic Pt cocatalyst. By contrast, molecular adsorption and activation of O_2 and H_2 on Pt_8O_8/TiO_2 become relatively difficult to occur. First, the adsorption of H_2 and O_2 on Pt_8O_8/TiO_2 is found to be much weaker, giving a value of 0.14 and 0.34 eV in terms of Gibbs free energy change, respectively. Second, their corresponding dissociations become difficult, being exothermic by only −0.13 eV ($O_2 + 2^* \rightarrow 2O^*$) and even endothermic by 0.02 eV ($H_2 + 2^* \rightarrow 2H^*$). More importantly, the dissociation barriers of O_2* and H_2* on Pt_8O_8/TiO_2 are also evidently

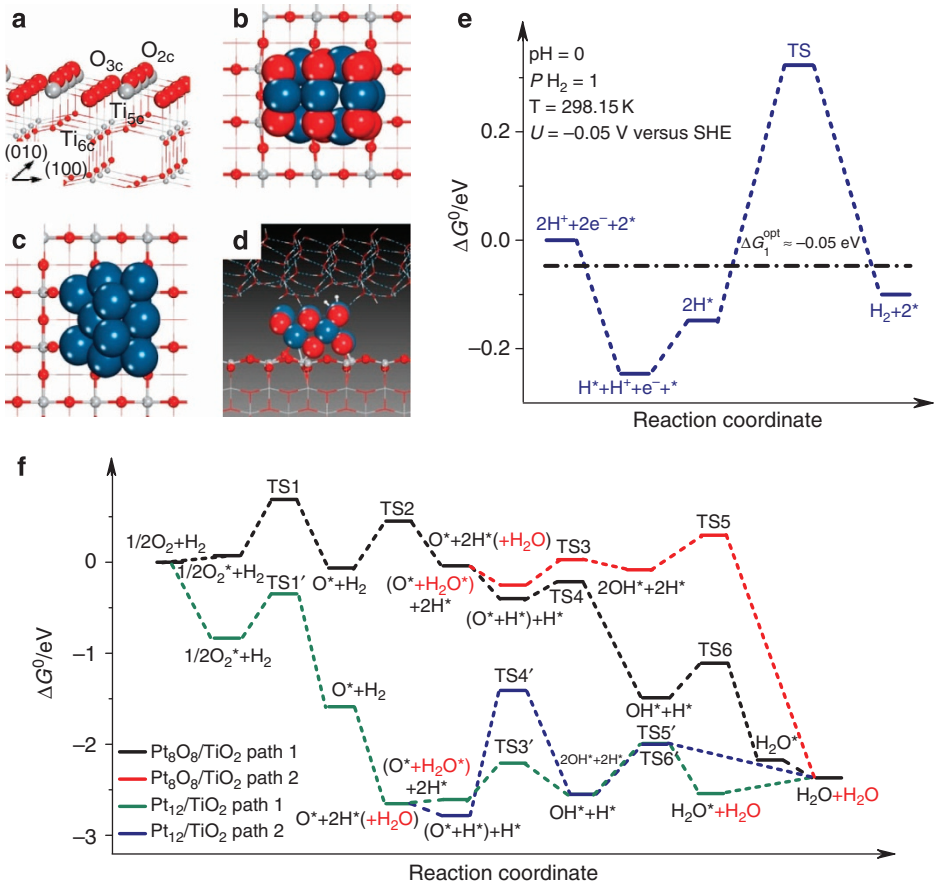

Figure 4 | Optimized structures and Gibbs free energy profiles. (**a**) Structure of anatase TiO_2(001) surface. (**b**) Optimized Pt_8O_8-cluster adsorbed on TiO_2(001) surface and (**c**) optimized Pt_{12}/TiO_2. (**d**) Transition state structure of H*–H* coupling on Pt_8O_8/TiO_2 in liquid phase, which contains two layers of water molecules above the Pt_8O_8-cluster. (**e**) Standard Gibbs free energy profile of HER in aqueous solution on Pt_8O_8/TiO_2. (**f**) Standard Gibbs free energy profile of H_2 reacting with O_2 on Pt_8O_8/TiO_2 and Pt_{12}/TiO_2 surfaces in gas phase. Dark blue balls represent Pt atoms, grey for Ti, white for H and red for O.

Table 1 | Reaction barriers and free energies*.

Reaction		Pt_8O_8/TiO_2		Pt_{12}/TiO_2	
		E_a	ΔG	E_a	ΔG
O_2 adsorption	$O_2 + ^* \rightarrow O_2^*$	/	0.14	/	−1.67
O_2^* dissociation	$O_2^* + ^* \rightarrow 2O^*$	0.62	−0.27	0.49	−1.51
H_2 adsorption	$H_2 + ^* \rightarrow H_2^*$	/	0.34	/	−1.06
H_2^* dissociation	$H_2^* + ^* \rightarrow 2H^*$	0.17	−0.32	/	
OH* formation	$O^* + H^* \rightarrow OH^* + ^*$	0.19	−0.92	1.38	0.14
	$O^* + H_2O^* \rightarrow 2OH^*$	0.28	0.17	0.40	0.06
H_2O^* formation	$OH^* + H^* \rightarrow H_2O^* + ^*$	0.38	−0.68	0.56	0.01
H_2O^* desorption	$H_2O^* \rightarrow H_2O + ^*$	/	−0.20	/	0.17

*The Gibbs free energy changes of H_2 and O_2 adsorption and H_2O desorption were calculated including the corresponding gas-phase entropy contributions under the standard state pressure and temperature. Calculated hydrogen oxidation reaction barriers and derived Gibbs free energy changes of the elementary reaction steps at anatase Pt_8O_8/TiO_2(001) and Pt_{12}/TiO_2(001) surfaces.

increased to 0.62 eV and 0.17 eV, respectively, indicating that activation of O_2/H_2 to generate surface H* and O* should be much more difficult on the Pt-oxide compared with metallic Pt cluster on TiO_2(001) surface. Thus, PtO-clusters cocatalyst presents a higher suppression ability relative to Pt-clusters in decomposing the evolved H_2 into H^+ and e^- reversely or activating the O_2 molecule, which is consistent with the experimental observation shown in Fig. 3.

To be systematic, the full reaction pathways of H_2O formation from the surface H* and O* catalysed by $Pt_{12}-$ and Pt_8O_8/TiO_2 were further investigated and compared. With respect to the formation of OH*, it is noteworthy that direct coupling of surface O* and H* to form OH* on Pt_{12}/TiO_2 needs to overcome a high barrier of 1.38 eV. Instead, OH* could be generated alternatively through O* reacting with an adsorbed H_2O^* molecule ($H_2O^* + O^* \rightarrow 2OH^*$), which has a much lower barrier (0.40 eV), whereas for OH formation on Pt_8O_8, this alternative pathway does not give evident facilitation because of an increased barrier of 0.28 eV relative to that (0.19 eV) in the direct O*–H* coupling. In other words, the OH* formation at Pt_8O_8/TiO_2 and Pt_{12}/TiO_2 could be achieved through different pathways, with the former being easier to occur (0.19 versus 0.40 eV; Fig. 4f). Further, the corresponding reaction barrier of OH* reacting with H* to form H_2O on Pt_8O_8/TiO_2 is calculated to be 0.38 eV, being a little

smaller than that (0.56 eV) on Pt_{12}/TiO_2. Overall, the step of surface intermediates H* and O* transforming into H_2O is easier to occur on Pt_8O_8/TiO_2 surface, in principle rationalized by the weak binding of H* and O* with the oxidized Pt. Nevertheless, from the Gibbs free energy profile of H_2 oxidation by O_2 on Pt_8O_8/TiO_2 and Pt_{12}/TiO_2 (Fig. 4f), one can see that the whole profile on Pt_{12}/TiO_2 is entirely below the initial state of the reactants, and also the profile on Pt_8O_8/TiO_2. Specifically, one can see that the rate-determining step in the whole process of both catalysts appears in the dissociation of O_2 based on the kinetic estimation, and the highest point (at the transition state of O_2 dissociation) in the favoured pathway on Pt_8O_8 (black line) is evidently higher than that of Pt_{12} (olive line) with a difference of $\sim$1 eV. Therefore, it can be understood that the reverse formation of H_2O through H_2 reacting with O_2 is favoured on metallic Pt-clusters; by contrast, H_2 oxidation can be efficiently suppressed on the oxidized PtO-clusters in the dark reaction because of the weak adsorption and dissociation ability of PtO-cluster towards O_2 and H_2 in principle.

Further, to confirm the reactivity of the H_2 back-reaction in methanol aqueous solution, DFT calculation was also carried out to demonstrate the relative suppressing ability of the oxidized Pt cluster and metallic Pt NPs (see details in Supplementary Fig. S21). Together with the '$H_2 + 1/2O_2 \rightarrow H_2O$' reaction addressed above, it can be concluded that no matter which form of possible back reactions, that is, '$1/2\,H_2 \rightarrow H^+ + e^-$', '$H_2 + 1/2O_2 \rightarrow H_2O$' or '$H_2 + HCHO \rightarrow CH_3OH$', the oxidized Pt_8O_8 cocatalyst exhibits a remarkable suppressing ability owing to the relatively difficult activation and dissociation of H_2 molecule.

In addition to the suppressing ability towards reverse reaction, the catalytic activity of the oxidized Pt species in catalysing HER ($H^+_{(aq)} + e^- + * \rightarrow 1/2\,H_2$) was also approximately estimated within the thermodynamics framework. By performing DFT calculation, thermodynamics of each elementary step of HER occurring on Pt_8O_8/TiO_2 in the water environment was calculated, in which the standard hydrogen electrode (SHE) was used as the reference to calculate the Gibbs free energy change (ΔG) of HER (see details in Methods). It indicated that there exists a volcano-shaped relation between the catalytic activity of HER and the Gibbs free energy change (ΔG_1) of the proton adsorption step ($H^+_{(aq)} + e^- + * \rightarrow H^*$) by applying the basic thermodynamic model[28], and our recent work showed that the maximum reaction rate of HER occurring on $Pt(O)/TiO_2$ catalysts could be arrived at the point of $\Delta G_1^{opt} = -0.05$ eV (unpublished results), which means ΔG_1 can be utilized as a measurement. On Pt_8O_8/TiO_2, ΔG_1 for the proton adsorption process were calculated to be -0.25 and 0.10 eV for the first and the second proton adsorption, respectively (see details in Supplementary Fig. S22 and Supplementary Table S5), both of which are close to the optimal adsorption strength ($\Delta G_1^{opt} = -0.05$ eV). Interestingly, ΔG_2 ($2\,H^* \rightarrow H_2 + 2^*$) was only 0.05 eV, showing the thermodynamic easiness of H* coupling into H_2. Further, we tried to locate the transition state for H*–H* coupling reaction (Fig. 4d), giving a reaction barrier as low as 0.47 eV. The standard Gibbs free energy profile of HER on Pt_8O_8/TiO_2 in the aqueous solution is illustrated in Fig. 4e, from which one can see that there is no evidently high point in the whole profile, suggesting the excellent performance of the oxidized Pt species (Pt_8O_8) in catalysing HER.

Discussion

In summary, PtO-clusters were found to have a pivotal role in unidirectional suppression of undesirable H_2 oxidation in photocatalytic water cleavage process. More importantly, these PtO-clusters can also demonstrate excellent efficiency in hydrogen evolution rate. Quantum chemical calculations have been applied to rationalize these experimentally observed structure–performance relations, and the origin of the promising performance of the oxidized Pt species in catalysing HER as well as suppressing unfavourable H_2 oxidation was also revealed. On the basis of experimental findings and theoretical models in this work, other high-efficient heterogeneous catalysts or catalytic systems might be developed for clean energy and environment applications.

Methods

Fabrication of photocatalysts. The $TiO_2\{001\}$ nanosheets and poly(methacrylic acid) polymer ligands were synthesized according to the literatures[29,30]. For PtO/TiO_2 photocatalyst, 50 mg of TiO_2 and 24.6 mg of polymer ligands were added into a screw-neck glass bottle (10 ml) containing chloroplatinic acid solution (5 ml, 0.2 mg ml^{-1}). After the solution becoming uniform by sonication, 0.5 ml of freshly prepared $NaBH_4$ aqueous solution (2 mg ml^{-1}) was rapidly injected into the solution under vigorous stirring (2,000 r.p.m.). After 2$\sim$3 h, another 0.5 ml of freshly prepared $NaBH_4$ solution was injected into the solution again. The stirring speed of the solution was kept at the same 2,000 r.p.m. for $>$10 h. In the washing process, the precipitate was sonicated for $>$2 min every time to ensure all photocatalyst dispersing uniformly in cleaning solution, and then separated by centrifuge. The precipitate was washed by deionized water for three times and ethanol for five times. After dried at room temperature, PtO/TiO_2 photocatalyst with clean surface was collected. The Pt/TiO_2 photocatalyst was synthesized using the similar process without adding the polymer ligands.

Photocatalysts characterization. The crystal structure was determined using X-ray diffraction (Bruker D8 Advanced Diffractometer with Cu K_α radiation). The molecular weight distribution of polymer ligands was measured by gel permeation chromatography (Waters). The detailed structural information of polymer ligands were analysed by Fourier transform infrared spectroscopy (Nicolet 5700) and NMR (Avance, 400 MHz) measurements. The loading amount of the cocatalysts was tested by ICP-atomic emission spectroscopy (Varian 710 ES). Further, the structure of the photocatalysts was examined by TEM (Tecnai 30, 300 kV). The chemical states of the elements in two photocatalytic systems were studied by XPS (Kratos Axis Ultra DLD), and the binding energy of the C 1*s* peak at 284.8 eV was taken as an internal reference.

Pt L_3-edge absorption spectra (EXAFS) were performed on the 1W2B beamline of the Beijing Synchrotron Radiation Facility, China, operated at $\sim$200 mA and $\sim$2.5 GeV. Pt foil and PtO_2 were used as reference samples and measured in the transmission mode, and the initial and used PtO/TiO_2 photocatalysts were measured in fluorescence mode. We used IFEFFIT software to calibrate the energy scale, to correct the background signal and to normalize the intensity.

Photocatalytic H_2 evolution test. The photocatalytic H_2 evolution test was carried out in a glass gas-closed-circulation system with a top irradiation-type reaction vessel (LabSolar H_2) and a 300-W xenon lamp (CEL-HXBF300). The temperature of reactant solution was maintained at 20 °C by a flow of cooling water during the test. Fifty milligrams of photocatalyst dispersed in solvent were added into the reaction vessel for photocatalytic H_2 evolution test. The amounts of evolved H_2 and O_2 were monitored by an online gas chromatograph (GC7890T). No air should be present in the system after evacuation by vacuum pump.

Theoretical calculation. All the spin-polarized calculations were performed with Perdew–Burke–Ernzerhof functional[31] within the generalized gradient approximation, in which the VASP package was used[32,33]. The project-augmented wave method was used to represent the core-valence electron interaction[34,35]. To model the anatase $TiO_2(001)$ surface, a three-layer $p(2 \times 2)$ slab (10.772×10.772 Å^2) corresponding to 48 TiO_2 units cell (144 atoms) was used, in which a vacuum layer of 15 Å was applied and the top layer of TiO_2 was allowed to relax. Because of the large size of the supercell, Monkhorst Pack mesh with Γ point *k*-point sampling in the surface Brillouin zone was used. For total energy calculations, the valence electronic states were expanded in plane wave basis sets with a cutoff energy of 450 eV. Atomic positions were relaxed until the absolute forces of each atom were $<$0.05 eV/Å.

Free energy calculation method. In the reaction of proton adsorbing and receiving excited electron, the proton–electron pair is always involved simultaneously in photocatalytic process. To obtain the free energy of the each elementary step, when involving $H^+ + e^-$, the SHE was used as the reference in standard Gibbs free energy calculation of HER[28]. Gibbs free energy changes of step (i) $H^+_{(aq)} + e^- + * \rightarrow H^*$ and (ii) $2\,H^* \rightarrow H_2 + 2^*$ (corresponding to ΔG_1 and

ΔG_2, respectively) can be calculated as follows:

$$\Delta G_1 = E_{ad}^{H} + \frac{1}{2}T\Delta S + eU - kT\ln C_{H^+} \quad (1)$$

$$\Delta G_2 = -2E_{ad}^{H} - T\Delta S + kT\ln P_{H_2} \quad (2)$$

in which U is the electronic voltage of an excited electron versus SHE (here it is at the conduction band bottom of anatase TiO_2), and therefore eU equals to -0.05 eV, whereas P_{H_2} and C_{H^+} are the relative partial pressure of H_2 in gas phase and the relative concentration of H^+ in the aqueous solution, respectively (see more details in Supplementary Note 3). The adsorption energy (E_{ad}^{H}) for H_2 was obtained from the DFT calculation at 0 K relative to the gas-phase H_2 molecule, which is defined as

$$E_{ad}^{H} = E_{H/sur} - E_{sur} - \frac{1}{2}E_{H_2} \quad (3)$$

where $E_{H/sur}$, E_{sur} and E_{H_2} are the total energy of the adsorption system, the clean surface and the H_2 molecule, respectively.

References

1. Fujishima, A. & Honda, K. Electrochemical photolysis of water at a semiconductor electrode. *Nature* **238,** 37–38 (1972).
2. Kudo, A. & Miseki, Y. Heterogeneous photocatalyst materials for water splitting. *Chem. Soc. Rev.* **38,** 253–278 (2009).
3. Chen, X., Shen, S., Guo, L. & Mao, S. S. Semiconductor-based photocatalytic hydrogen generation. *Chem. Rev.* **110,** 6503–6570 (2010).
4. Xing, J., Fang, W. Q., Zhao, H. J. & Yang, H. G. Inorganic photocatalysts for overall water splitting. *Chem. Asian J.* **7,** 642–657 (2012).
5. Bao, N., Shen, L., Takata, T. & Domen, K. Self-templated synthesis of nanoporous CdS nanostructures for highly efficient photocatalytic hydrogen production under visible light. *Chem. Mater.* **20,** 110–117 (2008).
6. Wang, X. *et al.* A metal-free polymeric photocatalyst for hydrogen production from water under visible light. *Nat. Mater.* **8,** 76–80 (2009).
7. Maeda, K., Higashi, M., Lu, D., Abe, R. & Domen, K. Efficient nonsacrificial water splitting through two-step photoexcitation by visible light using a modified oxynitride as a hydrogen evolution photocatalyst. *J. Am. Chem. Soc.* **132,** 5858–5868 (2010).
8. Chen, X., Liu, L., Yu, P. Y. & Mao, S. S. Increasing solar absorption for photocatalysis with black hydrogenated titanium dioxide nanocrystals. *Science* **331,** 746–750 (2011).
9. Xu, X., Randorn, C., Efstathiou, P. & Irvine, J. T. S. A red metallic oxide photocatalyst. *Nat. Mater.* **11,** 595–598 (2012).
10. Maeda, K. & Domen, K. Photocatalytic water splitting: recent progress and future challenges. *J. Phys. Chem. Lett.* **1,** 2655–2661 (2010).
11. Subbaraman, R. *et al.* Enhancing hydrogen evolution activity in water splitting by tailoring Li^+-$Ni(OH)_2$-Pt interfaces. *Science* **334,** 1256–1260 (2011).
12. Yoshida, M. *et al.* ATR-SEIRAS investigation of the Fermi level of Pt cocatalyst on a GaN photocatalyst for hydrogen evolution under irradiation. *J. Am. Chem. Soc.* **131,** 13218–13219 (2009).
13. Gray, H. B. Powering the planet with solar fuel. *Nat. Chem.* **1,** 7 (2009).
14. Grove, W. R. XXIV. On voltaic series and the combination of gases by platinum. *Philos. Mag.* **14,** 127–130 (1839).
15. Abe, R., Sayama, K. & Arakawa, H. Significant effect of iodide addition on water splitting into H_2 and O_2 over Pt-loaded TiO_2 photocatalyst: suppression of backward reaction. *Chem. Phys. Lett.* **371,** 360–364 (2003).
16. Maeda, K. *et al.* Noble-metal/Cr_2O_3 core/shell nanoparticles as a cocatalyst for photocatalytic overall water splitting. *Angew. Chem. Int. Ed.* **45,** 7806–7809 (2006).
17. Walsh, D., Arcelli, L., Ikoma, T., Tanaka, J. & Mann, S. Dextran templating for the synthesis of metallic and metal oxide sponges. *Nat. Mater.* **2,** 386–390 (2003).
18. Yang, H. G. *et al.* Anatase TiO_2 single crystals with a large percentage of reactive facets. *Nature* **453,** 638–641 (2008).
19. Knecht, J. & Stork, G. Röntgenphotoelektronen—spektroskopische untersuchung der thallium-oxidelektrode. *Fresenius Z. Anal. Chem.* **289,** 206 (1978).
20. Porsgaard, S. *et al.* Stability of platinum nanoparticles supported on SiO_2/Si(111): a high-pressure X-ray photoelectron spectroscopy study. *ACS Nano* **6,** 10743–10749 (2012).
21. Fu, Q., Saltsburg, H. & Flytzani-Stephanopoulos, M. Active nonmetallic Au and Pt species on ceria-based water-gas shift catalysts. *Science* **301,** 935–938 (2003).
22. Nomiyama, R. K., Piotrowski, M. J. & Da Silva, J. L. F. Bulk structures of PtO and PtO_2 from density functional calculations. *Phys. Rev. B* **84,** 100101 (2011).
23. Kondarides, D. I., Daskalaki, V. M., Patsoura, A. & Verykios, X. E. Hydrogen production by photo-induced reforming of biomass components and derivatives at ambient conditions. *Catal. Lett.* **122,** 26–32 (2008).
24. Ma, B. *et al.* The synergistic effects of two co-catalysts on Zn_2GeO_4 on photocatalytic water splitting. *Catal. Lett.* **134,** 78–86 (2010).
25. Croy, J. R. *et al.* Support dependence of MeOH decomposition over size-selected Pt nanoparticles. *Catal. Lett.* **119,** 209–216 (2007).
26. Völkening, S., Bedürftig, K., Jacobi, K., Wintterlin, J. & Ertl, G. Dual-path mechanism for catalytic oxidation of hydrogen on platinum surfaces. *Phys. Rev. Lett.* **83,** 2672–2675 (1999).
27. Michaelides, A. & Hu, P. Catalytic water formation on platinum: a first-principles study. *J. Am. Chem. Soc.* **123,** 4235–4242 (2001).
28. Nørskov, J. K. *et al.* Trends in the exchange current for hydrogen evolution. *J. Electrochem. Soc.* **152,** J23–J26 (2005).
29. Yang, X. H., Li, Z., Sun, C., Yang, H. G. & Li, C. Hydrothermal stability of {001} faceted anatase TiO_2. *Chem. Mater.* **23,** 3486–3494 (2011).
30. Li, Z., Tan, B., Allix, M., Cooper, A. I. & Rosseinsky, M. J. Direct coprecipitation route to monodisperse dual-functionalized magnetic iron oxide nanocrystals without size selection. *Small* **4,** 231–239 (2008).
31. Perdew, J. P., Burke, K. & Ernzerhof, M. Generalized gradient approximation made simple. *Phys. Rev. Lett.* **77,** 3865–3868 (1996).
32. Kresse, G. & Furthmüller, J. Efficiency of ab-initio total energy calculations for metals and semiconductors using a plane-wave basis set. *Comput. Mater. Sci.* **6,** 15–50 (1996).
33. Kresse, G. & Furthmüller, J. Efficient iterative schemes for ab initio total-energy calculations using a plane-wave basis set. *Phys. Rev. B* **54,** 11169–11186 (1996).
34. Blöchl, P. E., Jepsen, O. & Andersen, O. K. Improved tetrahedron method for Brillouin-zone integrations. *Phys. Rev. B* **49,** 16223–16233 (1994).
35. Kresse, G. & Joubert, D. From ultrasoft pseudopotentials to the projector augmented-wave method. *Phys. Rev. B* **59,** 1758–1775 (1999).

Acknowledgements

P.H. thanks the Chinese Government for the programme of 'Thousands Talents'. H.F.W. acknowledges the National Supercomputer Center in Jinan for computing time. This work was financially supported by National Natural Science Foundation of China (91022023, 21076076), SRF for ROCS, SEM, Programme for Professor of Special Appointment (Eastern Scholar) at Shanghai Institutions of Higher Learning, Major Basic Research Programme of Science and Technology Commission of Shanghai Municipality (10JC1403200), 111 project (B08021) and Australian Research Council's Future Fellowships (FT120100913).

Author contributions

H.G.Y. and H.F.W. conceived the project and contributed to the design of the experiments and computations, analysis of the data and revising the paper. Y.H.L. performed the photocatalyst preparation, characterizations and photocatalytic tests. J.X. and L.R.Z. performed measurements and data analyses of EXAFS. Y.H.L. and J.X. co-wrote the paper. Z.J.C. and H.F.W. conducted DFT calculations and wrote part of the paper (calculation). F.T. conducted the TEM and STEM examinations and contributed to writing the TEM and STEM sections. Z.L. and H.J.Z. carried out the preparation, measurements and data analyses of the polymer ligands PMAA. P.H. participated in a series of DFT investigations in the simulations of PtO/TiO_2 and Pt/TiO_2 photocatalysts and interpreted the computational data. H.G.Y. and H.F.W. contributed equally as senior authors. All the authors discussed the results and commented on the manuscript.

Additional information

Supplementary Information accompanies this paper at http://www.nature.com/naturecommunications

Competing financial interests: The authors declare no competing financial interests.

Reprints and permission information is available online at http://npg.nature.com/reprintsandpermissions/

How to cite this article: Li, Y. H. *et al.* Unidirectional suppression of hydrogen oxidation on oxidized platinum cluster. *Nat. Commun.* 4:2500 doi: 10.1038/ncomms3500 (2013).